Journal of
Applied Crystallography
ISSN 0021-8898

Received 28 May 2002
Accepted 10 October 2002

Numerical computation of critical properties and atomic basins from three-dimensional grid electron densities

C. Katan,[a] P. Rabiller,[a] C. Lecomte,[b] M. Guezo,[a] V. Oison[a] and M. Souhassou[b]*

[a]GMCM-UMR CNRS 6626, Université Rennes 1, av. Gal. Leclerc, 35042 Rennes, France, and [b]LCM3B-UMR CNRS 7036, Université Henri Poincaré Nancy 1, 54506 Vandoeuvre lès Nancy, France. Correspondence e-mail: souhas@lcm3b.uhp-nancy.fr

InteGriTy is a software package that performs topological analysis following the AIM (atoms in molecules) approach on electron densities given on three-dimensional grids. Tricubic interpolation is used to obtain the density, its gradient and the Hessian matrix at any required position. Critical points and integrated atomic properties have been derived from theoretical densities calculated for the compounds NaCl and TTF–2,5Cl_2BQ (tetrathiafulvalene–2,5-dichlorobenzoquinone), thus covering the different kinds of chemical bonds: ionic, covalent, hydrogen bonds and other intermolecular contacts.

1. Introduction

Nowadays, very accurate electron densities can be obtained both experimentally and theoretically. Experimental methods of recovering charge densities require high-resolution X-ray diffraction measurements on single crystals, which are analysed within the context of aspherical models. From the theoretical point of view, not only crystals but also molecules, clusters and surfaces can be tackled using either quantum-chemistry techniques, ranging from standard Hartree–Fock calculations to extremely accurate configuration-interaction methods, or techniques based on the density functional theory (DFT), which are increasingly used to perform *ab initio* calculations. Once the total electron density is known, it can be analysed in detail by means of its topological properties within the quantum theory of atoms in molecules (Bader, 1990, 1994). With such an analysis, one can go beyond a purely qualitative description of the nature and strength of interatomic interactions. It can also be used to define interatomic surfaces inside which atomic charges and moments are integrated.

The topological features of the total electron density $\rho(\mathbf{r})$ can be characterized by analysing its gradient vector field $\nabla\rho(\mathbf{r})$. Critical points (CPs) are located at points $\mathbf{b}_{\rm CP}$ where $\nabla\rho(\mathbf{r}_{\rm CP}) = 0$, and the nature of each CP is determined from the curvatures (λ_1, λ_2, λ_3) of the density at this point. The latter are obtained by diagonalizing the Hessian matrix $H_{ij} = \partial^2\rho(\mathbf{r})/\partial x_i \partial x_j$ ($i, j = 1, 2, 3$). Each CP is denoted by a pair of integers (ω, σ), where ω is the number of non-zero eigenvalues of the Hessian matrix $H(\mathbf{r})$ and σ is the sum of the signs of the three eigenvalues. In a three-dimensional stable structure, four types of CP can be found: (3, −3) peaks, corresponding to local maxima of $\rho(\mathbf{r})$, which occur at atomic nuclear positions and in rare cases at so-called non-nuclear attractors; (3, −1) passes, corresponding to saddle points where $\rho(\mathbf{r})$ is maximum in the plane defined by the axes corresponding to the two negative curvatures and minimum in the third direction (such bond critical points are found between pairs of bonded atoms); (3, +1) pales, where $\rho(\mathbf{r})$ is minimum in the plane defined by the axes associated with the two positive curvatures and maximum in the third direction (such ring critical points are found within rings of bonded atoms); (3, +3) pits, corresponding to local minima of $\rho(\mathbf{r})$. The numbers of each type of CP obey the following relationship depending on the nature of the system: N(peaks) − N(passes) + N(pales) − N(pits) = 0 or 1 for a crystal or an isolated system, respectively. The Laplacian of the electron density $\nabla^2\rho(\mathbf{r})$, which is given by the trace of $H(\mathbf{r})$, is related to the kinetic and potential electronic energy densities, $G(\mathbf{r})$ and $V(\mathbf{r})$, respectively, by the local Virial theorem

$$\tfrac{1}{4}\nabla^2\rho(\mathbf{r}) = 2G(\mathbf{r}) + V(\mathbf{r})$$

(atomic units, a.u., are used throughout the paper). The sign of the Laplacian at a given point determines whether the positive kinetic energy or the negative potential energy density is in excess. A negative (positive) Laplacian implies that density is locally concentrated (depleted). Within the quantum theory of atoms in molecules, a basin is associated to each attractor (3, −3) CP, defined as the region containing all gradient paths terminating at the attractor. The boundaries of this basin are never crossed by any gradient vector trajectory and satisfy $\nabla\rho(\mathbf{r}) \cdot \mathbf{N}(\mathbf{r}) = 0$, where $\mathbf{N}(\mathbf{r})$ is the normal to the surface at point $\mathbf{r}$. The corresponding surface is called the zero-flux surface and defines the atomic basin when the attractor corresponds to a nucleus. Only in very rare cases have non-nuclear attractors been evidenced (Madsen *et al.*, 1999). Within this space partitioning, the atomic charges deduced by integration over the whole basin are uniquely defined.

During the past 20 years, several programs have been developed to perform topological analysis of electron densities, but they are either connected to computer program packages (Gatti *et al.*, 1994; Koritsanszky *et al.*, 1995;

Souhassou *et al.*, 1999; Stash & Tsirelson, 2001; Stewart & Spackman, 1983; Volkov *et al.*, 2000) or have limitations concerning the type of wavefunctions used to determine $\rho(\mathbf{r})$ in *ab initio* calculations (Barzaghi, 2001; Biegler König *et al.*, 1982, 2001; Popelier, 1996) or to refine experimental data (Barzaghi, 2001). To our knowledge, only two procedures to analyse the topology of $\rho(\mathbf{r})$ numerically on grids have been described: Iversen *et al.* (1995) used a maximum entropy density, while Aray *et al.* (1997) sampled a theoretical density on a homogeneous grid. However, these approaches are limited to the determination of CPs. The present analysis of the topological features of total electron densities is independent of the way these densities are obtained and works for periodic and non-periodic systems. We show in this paper that this can be simply achieved by working with densities given on regular grids in real space. The developed software, *InteGriTy*, uses a tricubic Lagrange interpolation, which makes the CP search and integration method both accurate and fast. The densities used to illustrate the performance of our approach are theoretical *ab initio* densities obtained with the projector augmented wave (PAW) method (Blöchl, 1994).

The next section of this paper gives a short description of the method. Test compounds and computational details are given in §3. §4 is devoted to the determination of CPs and their characteristics, whereas §5 concerns the determination of atomic basins and charges. We will discuss the effect of grid spacing of the input density and the plane-wave cutoff used for the PAW calculations on the properties of different types of interactions (ionic, covalent and intermolecular).

2. Description of the method

2.1. Input data and interpolation

In order to achieve the topological analysis of any experimental or theoretical electron density, the density is given on a regular, not necessarily homogeneous grid in real space. A grid of stored values of $\rho(\mathbf{r})$ must be prepared, preferably in binary format in order to save disk space and with double precision to ensure high precision. The grid, which is defined by its origin, three mesh-grid vectors and the number of points in each grid direction, as well as atomic positions, must be specified with respect to a Cartesian coordinate system. Determination of the topological properties of $\rho(\mathbf{r})$ requires the knowledge of $\rho(\mathbf{r})$, $\nabla\rho(\mathbf{r})$ and $H(\mathbf{r})$ at many arbitrary points. This can be achieved in an accurate and efficient way by using a tricubic Lagrange interpolation (Press *et al.*, 1992). In one dimension, it uses values of ρ on two grid points on each side of the current point, as illustrated in Fig. 1. For a three-dimensional system, it uses 64 grid points surrounding the box containing the current point:

$$\rho(x, y, z) = \sum_{i=1}^{4}\sum_{j=1}^{4}\sum_{k=1}^{4} \rho(i, j, k)\, L_i(x)\, L_j(y)\, L_k(z).$$

As the first and second derivatives of this expression are straightforward, the evaluation of $\nabla\rho(\mathbf{r})$ and $H(\mathbf{r})$ is numerically very inexpensive. It is clear that with respect to analytical expressions, the interpolation may introduce errors. However, as shown in §§4 and 5, these errors are small for reasonable values of the grid interval size, and insignificant when compared with those resulting from the multipolar refinement of experimental structure factors. One should also note that this interpolation is not suitable for the topological analysis using $\nabla^2\rho(\mathbf{r})$ from the density. Higher order interpolation would be required or the Laplacian would have to be supplied on a grid.

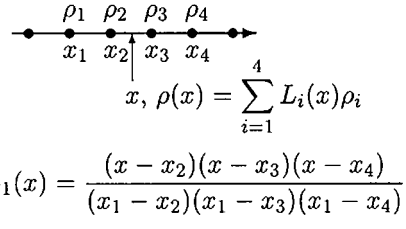

Figure 1
One-dimensional example for tricubic Lagrange interpolation. x_i and ρ_i are respectively the abscissa and density value at grid point i. The density at the current abscissa x is given by $\rho(x)$ where $L_i(x)$ are third-order polynomial, passing through all the grid points as shown by the example of $L_1(x)$.

2.2. Critical points

To locate the CPs, starting from every grid point, a standard Newton–Raphson technique (Press *et al.*, 1992) is used to find the zeros of its gradient modulus:

$$\mathbf{r}_{i+1} = \mathbf{r}_i - \alpha\, H^{-1}(\mathbf{r}_i) \cdot \nabla\rho(\mathbf{r}_i).$$

Far from the CPs, the full Newton step will not necessarily decrease the gradient modulus and the parameter α allows the step-size adjustment. In all our calculations, an α value of 0.3 led to stable results. This iterative procedure is used until the gradient modulus becomes less than a chosen threshold value. The corresponding CP is then stored if no other CP has been found in its vicinity. Otherwise, the program keeps the point that has the smallest gradient modulus. The CPs can then be classified with respect to their type and/or to the magnitude of $\rho(\mathbf{r}_{\rm CP})$. It is worth emphasizing that, since each grid point acts in its turn as a starting point, the CP search does not require *a priori* knowledge of atom location, nor the definition of plane or local coordinate systems. Periodic boundary conditions are used to treat periodic systems, whereas four grid points at each border of the input box are ignored in the case of non-periodic systems.

2.3. Atomic basins

Interpolation of electronic density on a grid can also be used to derive atomic basins and to integrate the density to obtain the atomic charges with good accuracy and within reasonable computer time. The surface S_Ω of each basin Ω is determined by its intersection with rays originating from the attractor. Only one intersection per ray is looked for. Then the determined surfaces may not be fully correct (Biegler König *et al.*, 1982; Popelier, 1998) but the missing volume that can be checked *a posteriori* is very low, thus having no appreciable

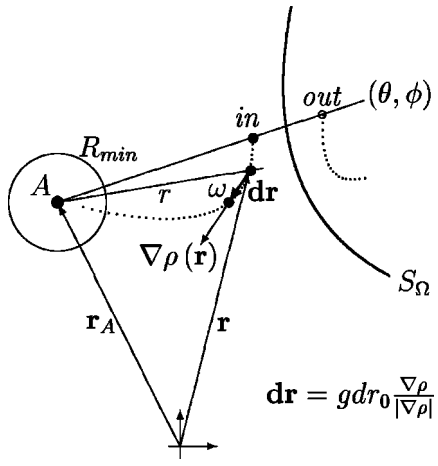

Figure 2
Schematic diagram to illustrate how a running point in radial coordinates is checked following the gradient path inside (filled circles) or outside (open circles) a basin centred on the attractor A and delimited by the surface S_Ω. $\mathbf{r}_A$ and $\mathbf{r}$ respectively give the positions of the attractor and the running point in the absolute Cartesian coordinate system. The incremental step length gdr_o is defined in the text.

effect on the integrated charges. A basin search is performed on the total density, whereas highly accurate integration is obtained from the valence part only, to avoid using unreasonably small grid steps. The program works with both periodic and non-periodic conditions for the input grids and a threshold electron density value can be applied to limit the surface of open systems (*e.g.* van der Waals envelope; Bader, 1990). The present integration results concern only periodic systems, thus allowing *a posteriori* validation of the process according to the sum over the whole unit cell of all basin volumes, including all atoms and possible non-nuclear attractors.

2.3.1. Basin search. To search for the surface of a basin, a radial coordinate system centred on each attractor is used and one point of the basin surface, $R_\Omega(\theta, \varphi)$, is looked for along the ray defined by the θ and φ angles. A point $r(\theta, \varphi)$ is declared inside the basin Ω if the following gradient path brings it towards a sphere centred on the attractor and with radius $R_{\min}$ small enough to be in the basin, as illustrated in Fig. 2. The running point is declared outside of Ω if a few iteration steps successively move it away from the attractor. The step amplitude used to follow the gradient is the product of a minimum step dr_0 weighted by a coefficient g depending on the angle ω between the considered ray and the gradient. It takes the form $\ln(g) = A|\cos(\Omega)|^B$ so that the maximum step size corresponds to the parallel situation. The search algorithm used for each ray is given in Fig. 3. A coarse bracketing, $R_{\text{low}} < R_\Omega(\theta, \varphi) < R_{\text{high}}$, is first performed, starting from the value R_{start} and using geometric progression with a common ratio $1 + \nu$. The sign and amplitude of ν depends on whether bracketing is performed downward to or away from the attractor. A dichotomy procedure is then used to refine the $R_\Omega(\theta, \varphi)$ value with predefined tolerance d_{tol}. At the first (θ, φ) step, R_{start} is set to an arbitrary value given for each atom as an input parameter. A crude estimation of a basin's limits is

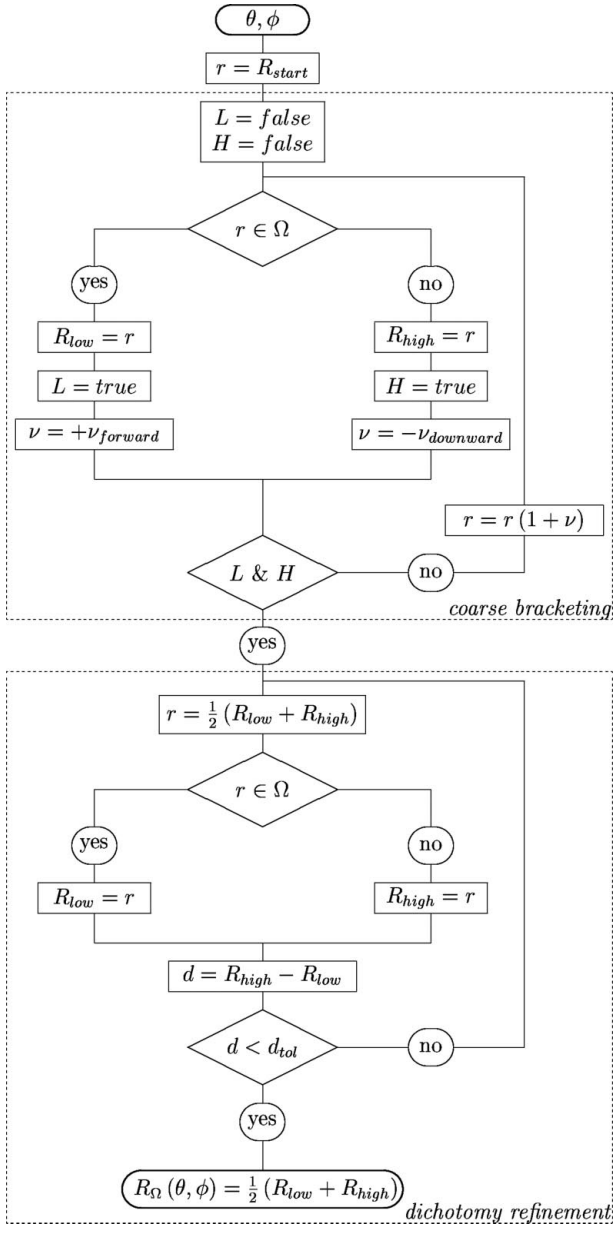

Figure 3
Basin surface location flowchart for a given ray originating from an attractor with spherical coordinates θ and φ. L and H are dummy logical constants to check if both the low and high limits of the coarse bracketing have been found. In the second part of the flowchart, the dichotomy process is stopped when the distance between the two limits is below the predefined tolerance d_{tol}.

performed first on a regular (θ, φ) grid with a small number of points n_θ and $n_\varphi = 2n_\theta$, with each $R_\Omega(\theta, \varphi)$ acting as a starting value for the next (θ, φ) step. This search is sufficient for graphical purposes and enables R_{start} initialization by linear interpolation at all (θ, φ) points added during the integration process. The $R_{\min}$ value is updated at the end of the crude estimation in order to save time during the integration process. It is automatically reset to a lower value when necessary.

2.3.2. Integration. Two methods can be used for integration, both using three nested integration 'do loops' with spherical

Table 1
Characteristics of crystalline NaCl critical points (CPs) for different grid spacings (Δr_{grid}) and numbers of plane waves (E_{cutoff}).

λ_1, λ_2 and λ_3 are the Hessian matrix eigenvalues. All values except E_{cutoff} are given in a.u.

Type	E_{cutoff}	Δr_{grid}	$\rho(\mathbf{r}_{CP})$	$\nabla^2\rho(\mathbf{r}_{CP})$	λ_1, λ_2, λ_3
(3, −1)	40 Ry	0.1564	0.0130	0.0577	−0.0122, −0.0119, 0.0817
NaCl	40 Ry	0.1138	0.0130	0.0576	−0.0122, −0.0121, 0.0820
	40 Ry	0.0939	0.0130	0.0571	−0.0122, −0.0121, 0.0814
	30 Ry	0.1138	0.0130	0.0581	−0.0123, −0.0121, 0.0825
	120 Ry	0.1138	0.0130	0.0583	−0.0123, −0.0121, 0.0827
(3, −1)	40 Ry	0.1138	0.0049	0.0127	−0.0024, −0.0011, 0.0163
ClCl					
(3, +1)	40 Ry	0.1138	0.0047	0.0134	−0.0025, 0.0035, 0.0124
(3, +3)	40 Ry	0.1138	0.0019	0.0056	0.0019, 0.0019, 0.0019

coordinates. The first one is straightforward and uses the same fixed number of (θ, φ, r) points for all attractors. The numbers n_r and n_θ of radial and θ steps are kept fixed, whereas the number $n_\varphi(\theta)$ of φ steps is θ dependent such that the elementary solid angle $\sin(\theta)\,\delta\theta\,\delta\varphi$ is constant. The integral Q_f of a quantity $f(\theta, \varphi, r)$ is simply given by the discrete sum

$$Q_f = \delta r\,\delta\theta \sum_{i=1}^{n_\theta} \sin(\theta_i)\,\delta\varphi(\theta_i) \sum_{j=1}^{n_\varphi(\theta_i)} \sum_{k=1}^{n_r} r_k^2 f(\theta_i, \varphi_j, r_k).$$

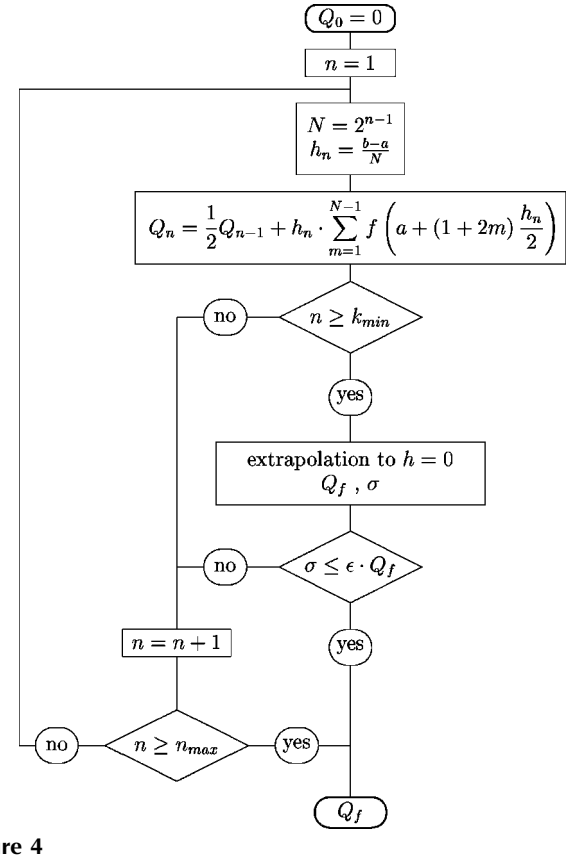

Figure 4
Romberg flowchart for the integration of a function f in the interval $[a, b]$. Q_f stands for an integrated property (charge, Laplacian, volume) at the three imbricated levels of integration, namely radial, φ and θ in the respective intervals $[0, R_\Omega(\theta, \varphi)]$, $[0, 2\pi]$ and $[0, \pi]$.

The second method uses the Romberg procedure (Press *et al.*, 1992) and is illustrated in Fig. 4 for a single variable function f integrated in the interval $[a, b]$. The procedure first calculates an estimation of the integral Q_f over n stages of the extended trapezoidal rule with successive integration steps $\{h_n\}$ and extrapolates Q_f with a k-order polynomial in h^2 to the continuum limit $h = 0$ over the last $n - k$ stages. The interpolation starts after $n \geq k_{min}$ stages. This iterative process is terminated when either an estimated error σ derived from the extrapolation operation yields a desired relative accuracy ε such that $\sigma \leq (\varepsilon Q_f)$, or a fixed maximum number of stages n_{max} is reached. Several convergence criteria can be used for the radial, φ and θ levels of integration. Total and valence atomic charges, volume and the Laplacian are integrated, and convergence criteria can be chosen on each of these quantities. Individual quantities are summed at the end of the loop over all attractors. The total charge and volume are then compared with the expected values and residuals are used to assess the accuracy of the integration process.

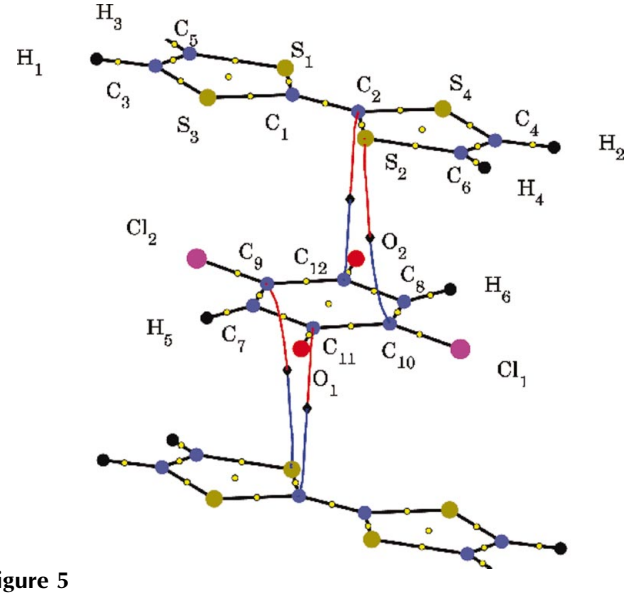

Figure 5
Representation of a mixed stack of alternating TTF and 2,5Cl_2BQ molecules, including atomic numbering. Open circles indicate bond and ring CPs. The lines connecting two molecules correspond to bond paths determined by following $\nabla\rho(\mathbf{r})$ with a small step size. Diamonds indicate some intermolecular (3, −1) CPs.

Table 2
Characteristics of the ring CP of 2,5Cl_2BQ and the $O_1\cdots H_3$ hydrogen bond of TTF–2,5Cl_2BQ for different E_{cutoff} and Δr_{grid} = 0.104 a.u.

Type	E_{cutoff}	$\rho(\mathbf{r}_{CP})$	$\nabla^2\rho(\mathbf{r}_{CP})$	λ_1	λ_2	λ_3
Ring CP	50 Ry	0.0210	0.1233	−0.0128	0.0613	0.0747
2,5Cl_2BQ	70 Ry	0.0209	0.1327	−0.0134	0.0664	0.0796
	90 Ry	0.0209	0.1314	−0.0131	0.0656	0.0789
	100 Ry	0.0209	0.1315	−0.0131	0.0656	0.0791
$O_1\cdots H_3$	50 Ry	0.0103	0.0359	−0.0106	−0.0102	0.0567
	70 Ry	0.0103	0.0384	−0.0109	−0.0103	0.0596
	90 Ry	0.0103	0.0375	−0.0108	−0.0103	0.0585
	100 Ry	0.0103	0.0370	−0.0107	−0.0103	0.0580

Table 3
Characteristics of the ring CP of 2,5Cl_2BQ and the $O_1\cdots H_3$ hydrogen bond of TTF–2,5Cl_2BQ for different Δr_{grid} and E_{cutoff} = 90 Ry.

Type	Δr_{grid}	$\rho(\mathbf{r}_{CP})$	$\nabla^2\rho(\mathbf{r}_{CP})$	λ_1	λ_2	λ_3
Ring CP	0.125	0.0209	0.1314	−0.0132	0.0656	0.0790
2,5Cl_2BQ	0.104	0.0209	0.1314	−0.0131	0.0656	0.0789
	0.085	0.0209	0.1313	−0.0131	0.0656	0.0788
$O_1\cdots H_3$	0.125	0.0103	0.0375	−0.0108	−0.0102	0.0585
	0.104	0.0103	0.0375	−0.0108	−0.0103	0.0585
	0.085	0.0103	0.0373	−0.0107	−0.0103	0.0584

Table 4
Characteristics of selected covalent-bond CPs of TTF–2,5Cl_2BQ for various E_{cutoff} and Δr_{grid} = 0.104 a.u.

Type	E_{cutoff}	$\rho(\mathbf{r}_{CP})$	$\nabla^2\rho(\mathbf{r}_{CP})$	λ_1	λ_2	λ_3
$C_{11}-O_1$	50 Ry	0.4038	0.6240	−1.0511	−0.9774	2.6526
	70 Ry	0.4070	0.3862	−1.0359	−0.9567	2.3788
	90 Ry	0.4079	0.3182	−1.0401	−0.9579	2.3162
	100 Ry	0.4079	0.3131	−1.0394	−0.9571	2.3096
C_6-S_2	50 Ry	0.2089	−0.3931	−0.3364	−0.2823	0.2256
	70 Ry	0.2094	−0.4185	−0.3370	−0.2835	0.2021
	90 Ry	0.2094	−0.4243	−0.3371	−0.2833	0.1961
	100 Ry	0.2094	−0.4251	−0.3371	−0.2833	0.1954
C_1-C_2	50 Ry	0.3410	−1.2044	−0.7568	−0.5956	0.1480
	70 Ry	0.3387	−1.0740	−0.7496	−0.5893	0.2649
	90 Ry	0.3388	−1.0786	−0.7453	−0.5853	0.2519
	100 Ry	0.3387	−1.0734	−0.7452	−0.5852	0.2570

3. Test compounds

Different types of crystals and molecules have been used to test the limits, accuracy and performance of the algorithm. In this paper, we have selected two crystals, namely NaCl, a classical example of an ionic crystal, and TTF–2,5Cl_2BQ, for covalent and intermolecular interactions. The latter compound was also chosen for the following reasons: with 26 atoms in the unit cell, the system is neither too small nor too large; as the unit cell is triclinic, the grid will not be orthogonal; the presence of inversion symmetry should be recovered in all properties; the expected small intermolecular charge transfer (about 0.5 out of 200 electrons) is a good quantity to test the accuracy of charge integration.

All calculations used to generate the electron densities were carried out with the projector augmented wave (PAW) method (Blöchl, 1994), an all-electron code developed by P. E. Blöchl. The wavefunctions were expanded into augmented plane waves up to a kinetic energy E_{cutoff} ranging from 30 to 120 Ry.

Table 5
Characteristics of selected covalent-bond CPs of TTF–2,5Cl_2BQ for various Δr_{grid} and E_{cutoff} = 90 Ry.

Type	Δr_{grid}	$\rho(\mathbf{r}_{CP})$	$\nabla^2\rho(\mathbf{r}_{CP})$	λ_1	λ_2	λ_3
C_{11}–O_1	0.125	0.4080	0.2268	−1.0899	−1.0180	2.3347
	0.104	0.4079	0.3182	−1.0401	−0.9579	2.3162
	0.085	0.4079	0.2913	−1.0266	−0.9879	2.3058
C_6-S_2	0.125	0.2095	−0.4207	−0.3353	−0.2824	0.1970
	0.104	0.2094	−0.4243	−0.3371	−0.2833	0.1961
	0.085	0.2095	−0.4239	−0.3369	−0.2835	0.1965
C_1-C_2	0.125	0.3388	−1.0770	−0.7438	−0.5841	0.2509
	0.104	0.3388	−1.0786	−0.7453	−0.5853	0.2519
	0.085	0.3388	−1.0804	−0.7462	−0.5862	0.2520

NaCl was treated within a face-centred cubic (f.c.c.) cell with a = 10.62 a.u. and eight **k** points in reciprocal space. For TTF–2,5Cl_2BQ, we used the experimental geometry at ambient conditions (Girlando *et al.*, 1993). The unit cell is triclinic (a = 14.995, b = 13.636, c = 12.933 a.u., α = 106.94, β = 97.58, γ = 93.66°) and contains one TTF and one 2,5Cl_2BQ molecule, both on inversion centres. These molecules are respectively electron donor and acceptor molecules, alternating along the **b** axis to form mixed stacks (Fig. 5). The *ab initio* calculations were performed with three **k** points between γ and $Y = \frac{1}{2}\mathbf{b}^*$ in the Brillouin Zone (Katan *et al.*, 1999).

4. Critical points

4.1. Ionic bonds

NaCl presents four types of different CPs, as shown in Fig. 6. Within the unit cell there are six (3, −1) CPs between Na and Cl, six (3, −1) CPs between Cl and Cl, surrounded in the Na$\cdots$Na direction by twelve (3, +1) CPs, two (3, +3) CPs and

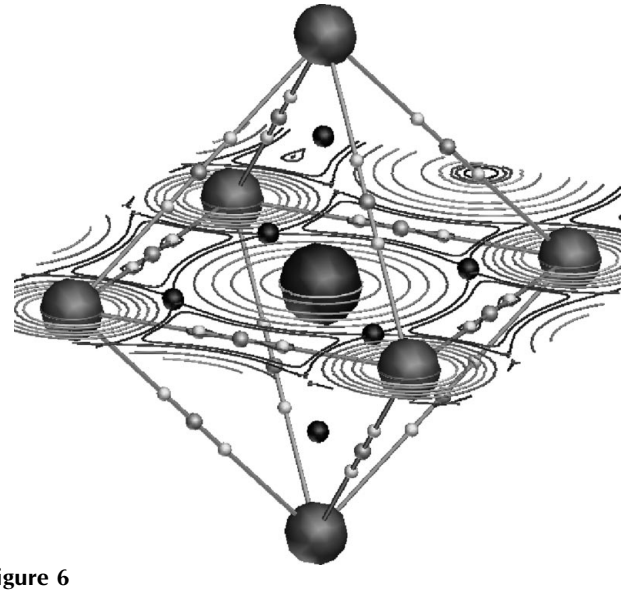

Figure 6
Octahedron with one Cl at its centre and six Na at its vertices. Iso-density curves are represented in the plane of the Na$\cdots$Cl nearest neighbours. The six dark spheres correspond to the (3, −1) CPs between Na and Cl, the 12 grey spheres correspond to the (3, −1) CPs between Cl and Cl, and the lightest smallest spheres correspond to the (3, +1) CPs. The (3, +3) CPs are not shown here.

Table 6
NaCl integration results *versus* Δr_{grid} with E_{cutoff} = 120 Ry.

	Δr_{grid}			
	0.095	0.0885	0.08	0.063
ΔN	0.0362	0.0289	0.0198	0.0086
δN	0.0367	0.0285	0.0199	0.0090
ΔV	0.095	0.096	0.020	0.090
q_{Na}	0.8282	0.8282	0.8188	0.8283
v_{Na}	63.36	63.36	63.29	63.36
q_{Cl}	−0.8648	−0.8572	−0.8387	−0.8373
v_{Cl}	236.18	236.18	236.17	236.17
CT	0.85	0.84	0.83	0.83
σ_{CT}	0.04	0.03	0.02	0.01

Table 7
TTF–2,5Cl_2BQ integration results *versus* E_{cutoff} with Δr_{grid} = 0.104 a.u.

	E_{cutoff} (Ry)			
	50	70	90	100
ΔN	−0.006	−0.005	−0.006	−0.006
δN	0.066	0.022	0.020	0.020
ΔV	−0.92	−1.44	−1.93	−1.89
q_{TTF}	0.455	0.453	0.452	0.453
$q_{2,5Cl_2BQ}$	−0.522	−0.475	−0.472	−0.473
CT	0.49	0.46	0.46	0.46
σ_{CT}	0.07	0.02	0.02	0.02

two nuclear attractors. The characteristics of these CPs are given in Table 1 along with the variation of CP properties *versus* grid spacing (Δr_{grid}) and number of plane waves (E_{cutoff}) for only one representative CP, all other CPs presenting even smaller variations. These results show that a grid spacing of about 0.15 a.u. and a plane-wave cutoff of 30 Ry are sufficient to achieve accurate results for this ionic compound.

4.2. Molecular compounds

Low densities at critical points are observed in the crystal of TTF–2,5Cl_2BQ in interaction regions. Two examples are shown in Tables 2 and 3, corresponding to the ring CP of 2,5Cl_2BQ and to the strongest hydrogen bond occurring in the plane shown in Fig. 7. In both cases, the smallest E_{cutoff} (50 Ry) and the largest grid spacing (0.125 a.u.) already give quite good results. These properties converge even better for all other low-density CPs. As for ionic bonding, even smaller E_{cutoff} and large Δr_{grid} can be used since the electron density is particularly smooth close to the CPs. The situation is much different for covalent bonds where $\rho(\mathbf{r}_{CP})$ is much higher and the electron density varies more rapidly. All covalent-bond CPs have been plotted in Fig. 5. Typical covalent bonds of TTF–2,5Cl_2BQ are summarized in Tables 4 and 5 for different E_{cutoff} and Δr_{grid}. For most bonds, the CP properties do not vary too much, except for the C═O bond where the low E_{cutoff} gives a value of $\nabla^2\rho(\mathbf{r}_{CP})$ that is twice as large as the values at higher E_{cutoff}. This is due the rapid change in the electron density along the bond path. For this reason, the C═O bond properties are also the most sensitive to Δr_{grid} (Table 5). This makes the problem particularly difficult to treat. Evidently, accurate CP characteristics of simple bonds are more readily obtainable than those of double bonds.

Finally, we have checked in each case that CPs which are equivalent by symmetry are equivalent at least within the numbers of digits indicated in the different tables of this section. All these results clearly show that CP properties can easily be deduced from densities given on regular grids, the choice of the grid step size depending on the nature of the bonds of interest.

5. Atomic basins

The accuracy of integration from a grid density not only depends on the integration method and on the way of determining the basin surfaces, but also on the accuracy of the electron density data at the grid points, on the degree of missing information due to grid spacing, and on the possible bias introduced by the interpolation procedure. The following residuals have been defined to estimate the accuracy of the integration process: N_{grid} is the number of electrons in the unit cell obtained over all elementary volume units, either by discrete summation or by using an analytical integral expression of the tricubic interpolation. Then $\Delta N = N_{grid} - N_{real}$ is the difference between the number of valence electrons obtained by integration over the whole unit cell and its expected real value. The quantities v_Ω and S_Ω respectively refer to the volume and surface of the basin Ω. The number of electrons in an individual basin is denoted n_Ω. $\delta N = \sum n_\Omega - N_{real}$ is the residual after summation over all atomic basins. The basin volume uncertainty is set equal to the product of the tolerance d_{tol} and an estimation of the atomic surface S_Ω. The total volume uncertainty is given by $\sigma_V = d_{tol}\sum S_\Omega$ and the

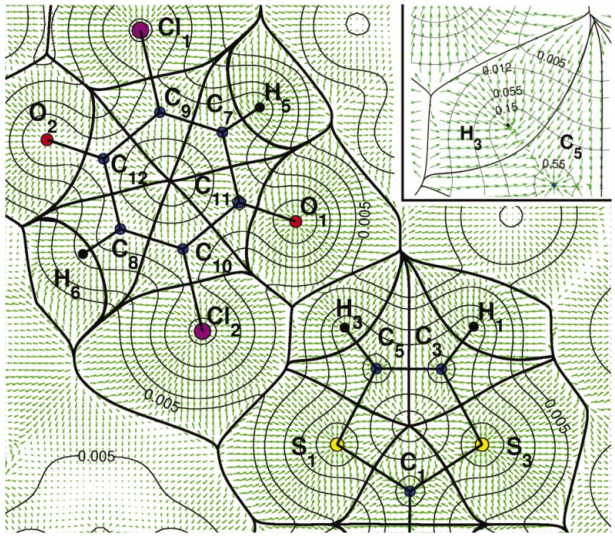

Figure 7
Representation of atomic basins in the plane containing both the TTF and the 2,5Cl_2BQ molecules. The strongest hydrogen bond in the TTF–2,5Cl_2BQ crystal occurs between O_1 and H_3. The arrows indicate the direction and magnitude of the gradient in the plane. An example of a small unreachable volume due to multiple intersection of the atomic surface with a ray originating from atom C_5 can be seen in the top right of the figure.

Table 8
Sets of tested parameters and results for Romberg integration on the charge-transfer crystal TTF–2,5Cl_2BQ.

The cell volume is V_{cell} = 2493.062 a.u. Direct integration of valence electron density over the whole unit cell gives an input error $\Delta N = -0.0056$ electron. Δr_{grid} = 0.104 a.u.; E_{cutoff} = 90 Ry.

Basin search						
$dr_o = d_{tol}$	5×10^{-2}	5×10^{-3}	10^{-3}	5×10^{-4}	5×10^{-4}	10^{-4}
A	5	50	250	500	500	2500
B	0.5	0.5	0.5	1	1	1
Romberg						
k_{min}	4	6	6	6	6	6
ε_r	10^{-3}	10^{-3}	5×10^{-4}	10^{-4}	2×10^{-7}	10^{-7}
ε_φ	10^{-2}	10^{-2}	5×10^{-3}	10^{-3}	8×10^{-5}	10^{-5}
ε_θ	5×10^{-2}	5×10^{-2}	10^{-2}	10^{-3}	5×10^{-5}	10^{-4}
CPU time	23 s	104 s	222 s	19 min	3.5 h	43 h
δN	−0.413	0.080	0.056	0.019	0.014	0.006
ΔV	18.98	−1.88	−0.98	−1.56	−0.77	−1.11
σ_V	120	12	2.4			
1.25	1.2	0.2				
q_{TTF}	0.862	0.424	0.434	0.448	0.454	0.455
$q_{2,5Cl_2BQ}$	−0.448	−0.503	−0.490	−0.467	−0.468	−0.461
CT	0.65	0.46	0.46	0.46	0.461	0.458
σ_{CT}	0.40	0.08	0.06	0.02	0.015	0.006
C_1						
$n_{\theta,\varphi}$	89	1089	1089	1441	8639	38081
$\bar{n}_r$	15	33	33	56	212	258
q	−0.311	−0.285	−0.285	−0.283	−0.284	−0.284
v	69.11	65.96	65.96	65.50	65.56	65.56
S_1						
$n_{\theta,\varphi}$	81	1089	1089	1089	2591	8513
$\bar{n}_r$	23	33	40	61	292	373
q	0.249	0.252	0.255	0.258	0.258	0.258
v	183.22	181.86	181.84	181.95	182.21	182.18

residual volume error by $\Delta V = \sum v_\Omega - V_{cell}$. If the uncertainty σ_V is found to be clearly less than the residual ΔV, the question arises about the way the atomic surfaces are derived. In this case, either there are several intersections of the basin surface with one ray originating from the attractor, or the parameters used to follow the gradient path have to be modified, or some attractors are missing in the input list. Finally, the largest charge difference between symmetry-equivalent atoms, the intra- or intermolecular charge transfer (CT) and its estimated uncertainty (σ_{CT}) are the other criteria which can be used as a measure of the accuracy of the integration process.

5.1. Grid spacing and *ab initio* calculation convergence

In the case of NaCl, *ab initio* calculations are not too sensitive to the convergence criterion E_{cutoff}, so the grid-spacing effect can clearly be evidenced. Well converged integration results using the Romberg procedure are given in Table 6. One can see that the electron number residual δN after integration and summation over all basins is very close to ΔN, given as input. This residue monotonically decreases with reducing grid spacing, whereas the volume residual ΔV is almost constant. A reasonable estimation of interatomic charge transfer can be derived from the valence density within a precision of 0.01 electron for a grid spacing of about 0.06 a.u. The prohibitive grid spacing required to obtain the charge transfer with the same precision from the total density can be estimated to 0.03 a.u., as illustrated in Fig. 8.

In the case of molecular crystals, which exhibit short bonds with large and quickly varying electron density at their bond critical points, such as C═O, the *ab initio* calculations are more sensitive to the convergence criterion E_{cutoff} defining the plane-wave expansion basis set. This is found in the integration results, as illustrated in Table 7 for TTF–2,5Cl_2BQ, where the electron number residual δN after integration over all atomic basins is slightly different from that after direct summation over the unit cell ΔN. This may arise from the larger number of atoms and from the less smooth shapes of the atomic basins (Fig. 9) in comparison with the NaCl case. Nevertheless, using E_{cutoff} above 50 Ry is enough to obtain the intermolecular charge transfer within 0.02 electron precision, which is the goal that originally motivated this work.

5.2. Romberg *versus* fixed spherical grid integration

Different sets of parameters for the Romberg integration procedure, including adequate parameters for the basin-limits search, are given in Table 8. The indicated CPU time corresponds to a PC with an 800 MHz processor and 512 MB RAM, and does no include the time spent reading the density files or performing the direct unit-cell summation. The preliminary

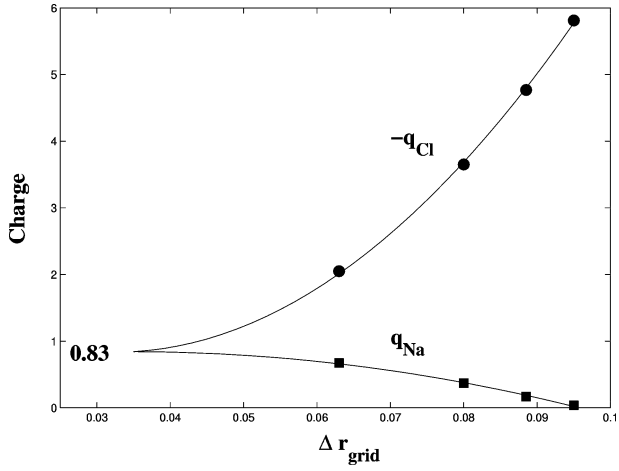

Figure 8
NaCl atomic charges from the total electron density *versus* grid spacing. Solid lines are guides to the eye, converging at the 0.83 charge transfer estimated from valence-density considerations.

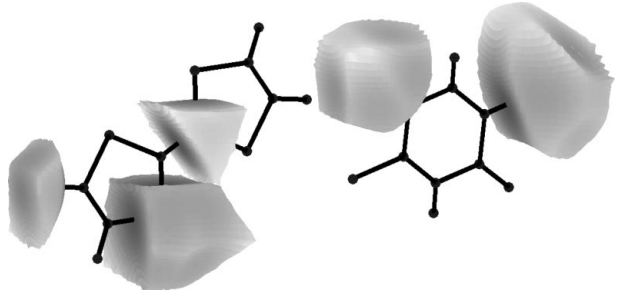

Figure 9
Three-dimensional representation of some atomic basins in the TTF–2,5Cl_2BQ charge-transfer complex.

estimation of basin envelopes is performed with $n_\theta = 18$ and $n_\varphi = 36$, using a tolerance $d_{\rm tol} = 0.05$ a.u. This operation takes about 0.8 s per basin. The integration convergence criteria have been applied only to the volume and the valence density, since the grid spacing used may not correctly restore density cusps near atomic nuclei. Obtaining the intermolecular charge transfer, in the case of TTF–2,5Cl_2BQ, within a precision of about one hundredth of an electron takes about 1 min per basin. The weaker criteria, although leading to an unsatisfactory residual from the point of view of intermolecular charge transfer, nevertheless give a good indication of atomic charges within less than 1 s per basin. The residual volume error remains of the order of one cubic a.u. out of nearly 2500 a.u. for the unit cell, and only for the more severe integration convergence criteria may the problem of very precise determination of basin boundaries appear (Fig. 7). The greatest discrepancy between charges obtained for equivalent atoms ranges from 10^{-4} for the set of parameters leading to the best integration, to 10^{-3} for the set giving the shorter CPU times. For comparison, integration has been performed using a fixed spherical grid for all basins. The corresponding parameters and results are listed in Table 9. The total number of angular loops is denoted $n_{\theta,\varphi}$. Below $n_{\theta,\varphi} n_r \simeq 10^4$ integration points, no realistic atomic charges can be obtained. Indeed, the very short time that can be used with Romberg integration comes from its internal k-order polynomial extrapolation, which gives an error estimate of the order of $O(1/N^{2k})$ instead of $O(1/N^2)$ for the simple discrete summation with the same number N of integration points.

In the case of fixed spherical grid integration, compared with Romberg integration, the volume uncertainty is in most of the cases greater than the residual volume error, thus giving no information about missing or overlapping volumes. The discrepancy between charges of equivalent atoms is also about an order of magnitude higher. The point that makes the Romberg procedure more favourable is that the number of integration points is automatically adapted to each basin to the desired level of convergence, as illustrated for atoms C_1 and S_1 in Table 8, whereas taking a fixed mean spherical grid leads to missing or biased information for some atoms and adds unnecessary points for other ones. The number $\bar{n}_r$ of radial loops indicated in Table 8 is the average over all angular loops for each basin.

Table 9
Sets of tested parameters and results for fixed spherical grid integration on TTF–2,5Cl_2BQ.

Basin search				
$dr_o = d_{\rm tol}$	5×10^{-3}	5×10^{-3}	5×10^{-4}	5×10^{-4}
A	50	50	500	500
B	0.5	0.5	0.5	1
Spherical grid				
n_θ	18	30	50	72
$n_{\theta,\varphi}$	406	1134	3162	6574
n_r	30	50	100	240
CPU time	53 s	135 s	20 min	2.2 h
$\delta N^{\rm tot}$	1.534	−0.192	−0.204	−0.227
$\delta N^{\rm val}$	0.147	0.061	0.041	0.025
ΔV	−30.50	−2.18	−0.27	−0.35
$\sigma_{\rm CT}$	12.5	11	1.2	1.2
$q_{\rm TTF}$	0.398	0.433	0.442	0.449
$q_{2,5Cl_2BQ}$	−0.545	−0.494	−0.484	−0.474
CT	0.47	0.46	0.46	0.46
$\sigma_{\rm CT}$	0.15	0.06	0.04	0.03
C_1				
q	−0.286	−0.284	−0.285	−0.284
v	65.14	65.52	65.59	65.55
S_1				
q	0.251	0.254	0.256	0.257
v	181.96	182.21	182.20	182.23

6. Conclusion

We have shown that topological properties can be derived from electron densities given on three-dimensional grids by using tricubic interpolation to extract the density, its gradient and the Hessian matrix at any given position. Except for very short covalent bonds, such as C═O, critical-point properties can be obtained with a grid spacing of about 0.1 a.u. The same grid spacing can also be used to obtain atomic charges with highly accurate values by integration over atomic basins using the valence electron density. The integration is performed with a spherical coordinate system centred on the attractors and uses the robust Romberg algorithm, which allows the number of integration points to be automatically adapted for each basin and offers the choice between saving computing time or giving preference to accuracy.

This work has benefited from collaborations within the Ψ_k-ESF Research Program and the Training and Mobility of Researchers Program 'Electronic Structure' (Contract: FMRX-CT98-0178) of the European Union and the International Joint Research Grant 'Development of Charge Transfer Materials with Nanostructures' (Contract: 00MB4). Parts of the calculations were supported by the 'Centre Informatique National de l'Enseignement Supérieur' (CINES, France). We would like to thank P. E. Blöchl for his PAW code and P. Sablonniere for useful discussions.

References

Aray, Y., Rodríguez, J. & Rivero, J. (1997) *J. Phys. Chem.* A**101**, 6976–6982.
Bader, R. F. W. (1990). *Atoms in Molecules: a Quantum Theory. The International Series of Monographs on Chemistry*. Oxford: Clarendon Press.
Bader, R. F. W. (1994). *Phys. Rev. B*, **49**, 13348–13356.
Barzaghi, M. (2001). *PAMoC* (Version 2001.0), *Online User's Manual*, Centro del CNR per lo Studio delle Relazioni tra Struttura e Reattività Chim, Milano, Italy. (http://www.csrsrc.mi.cnr.it/ barz/pamoc/.).
Biegler König, F. W., Bader, R. F. W. & Tang, T. (1982). *J. Comput. Chem.* **3**, 317–328. (*AIMPAC* interfaced to *GAUSSIAN*, http://www.chemistry.mcmaster)
Biegler König, F. W., Schönbohm, J. & Bayles, D. (2001). *J. Comput. Chem.* **22**, 545–559. (*AIM2000*, http://www.aim2000.de/mcmaster.ca/aimpac.)
Blöchl, P. E. (1994). *Phys. Rev. B*, **50**, 17953–17979.
Gatti, C. (1996). *Acta Cryst.* A**52**, C-555–C-556. (*TOPOND* interfaced to *CRYSTAL*.)
Gatti, C., Saunders, V. R. & Roetti, C. (1994). *J. Chem. Phys.* **101**, 10686–10696.
Girlando, A., Painelli, A., Pecile, C., Calestani, G., Rizzoli, C. & Metzger, R. M. (1993). *J. Chem. Phys.* **98**, 7692–7698.

Iversen, B. B., Larsen, F. K., Souhassou, M. & Takata, M. (1995). *Acta Cryst.* B**51**, 580–591.
Katan, C. & Koenig, C. (1999). *J. Phys. Condens. Matter*, **11**, 4163–4177.
Koritsanszky, T., Howard, S., Richter, T., Su, Z., Mallinson, P. R. & Hansen, N. K. (1995). *XD Computer Program Package for Multipolar Refinement and Analysis of Electron Densities from X-ray Diffraction Data*. Program *XDPRO*. Free University of Berlin, Germany.
Madsen, G. K. H., Gatti, C., Iversen, B. B., Damjavonic, Lj., Stucky, G. D. & Srdanov, V. I. (1999). *Phys. Rev. B*, **59**, 12359–12369, and references therein.
Popelier, P. L. A. (1996). *Comput. Phys. Commun.* **93**, 212–240. (*MORPHY98*, http://morphy.uk/ch.umist.ac.uk/.)
Popelier, P. L. A. (1998) *Comput. Phys. Commun.* **108**, 180–190.
Press, W. H., Teukolsky, S. A., Vetterling, W. T. & Flannery, B. P. (1992). *Numerical Recipes – The Art of Scientific Computing*, 2nd ed. Cambridge University Press.
Souhassou, M. & Blessing, R. H. (1999). *J. Appl. Cryst.* **32**, 210–217. (*NEWPROP* interfaced to *MOLLY.)*
Stash, A. & Tsirelson, V. (2001). *WINPRO – A Program for Calculation of the Crystal and Molecular Properties Using the Model Electron Density*, http://stash.chat.ru.
Stewart, R. F. & Spackman, M. A. (1983). *VALRAY User's Manual*. Carnegie-Mellon University, Pittsburgh, USA.
Volkov, A., Gatti, C., Abramov, Y. & Coppens, P. (2000). *Acta Cryst.* A**56**, 252. (*TOPXD* interfaced to *XD*, http://harker.chem.buffalo.edu/public/topxd/.)